Universal ac conduction in large area atomic layers of CVD-grown MoS_2

S. Ghosh,[1] S. Najmaei,[2] S. Kar,[3] R. Vajtai,[2] J. Lou,[2] N. R. Pradhan,[4] L. Balicas,[4] P. M. Ajayan,[2] and S. Talapatra[1]
[1]*Department of Physics, Southern Illinois University, Carbondale, Illinois 62901, USA*
[2]*Department of Mechanical Engineering and Materials Science, Rice University, Houston, Texas 77005, USA*
[3]*Department of Physics, Northeastern University, Boston, Massachusetts 02115, USA*
[4]*National High Magnetic Field Laboratory, Florida State University, Tallahassee, Florida 32310, USA*
(Received 20 August 2013; published 19 March 2014)

Here, we report on the ac conductivity [$\sigma'(\omega)$; 10 mHz $< \omega <$ 0.1 MHz] measurements performed on atomically thin, two-dimensional layers of MoS_2 grown by chemical vapor deposition (CVD). $\sigma'(\omega)$ is observed to display a "universal" power law, i.e., $\sigma'(\omega) \sim \omega^s$ measured within a broad range of temperatures, 10 K $< T <$ 340 K. The temperature dependence of "s" indicates that the dominant ac transport conduction mechanism in CVD-grown MoS_2 is due to electron hopping through a quantum mechanical tunneling process. The ac conductivity also displays scaling behavior, which leads to the collapse of the ac conductivity curves obtained at various temperatures into a single master curve. These findings establish a basis for our understanding of the transport mechanism in atomically thin, CVD-grown MoS_2 layers.

DOI: 10.1103/PhysRevB.89.125422 PACS number(s): 72.20.−i, 63.22.Np, 71.23.−k, 72.80.Ng

Van der Waals bonded layered solids such as MoS_2, WS_2, $MoSe_2$, *h*-BN, etc. have emerged as the materials of choice for obtaining atomically thin, two-dimensional (2D) systems [1–4] with fascinating electrical as well as optical properties [5–10]. Field-effect transistors composed of a single, or few layers of MoS_2 were found to display high electron mobilities, making them potentially useful as active elements in thin-film transistors [1,8–10]. These observations, coupled with the fact that single-layer MoS_2 is a direct-band-gap material ($\sim$1.8 eV), in contrast to its bulk counterpart which is an *n*-type semiconductor with an indirect band gap of $\sim$1.3 eV, stimulated intensive research on the electrical and optoelectronic properties of single-layer MoS_2 transistors [3–7].

Such observations, mostly on mechanically exfoliated layers of MoS_2 from single crystals, provided enough impetus to explore innovative methods for large-scale synthesis of atomically thin MoS_2 layers [3,11–15]. Among these, liquid phase exfoliation [3,11], laser thinning [12], as well as the chemical vapor deposition (CVD) method [13–15] are now being utilized to synthesize large-scale area MoS_2 layers. However, the materials produced using these techniques are, in general, susceptible to structural disorder [16,17]. Such disorder is known to affect the properties of the material; for example, in semiconductors, atomic defects and bonding disorder influence their band structure, which in turn influences their charge transport [18,19] properties. Therefore, understanding the correlation between the structure and physical properties of these materials is of fundamental interest. In particular, studying the electrical conduction mechanisms [20–28] of 2D layered solids is of major importance, since it would play a relevant role in many of the envisioned optoelectronic applications based on these materials.

In recent times a large body of research has been exploring the exciting electronic properties of CVD-grown MoS_2 layers, revealing rich new science and its technological potential. A question of fundamental importance then arises with regard to how the electrical performance of these materials will compare with their crystalline counterparts. In this paper, we present a study on the electrical conduction mechanisms of large area, atomically thin CVD-grown MoS_2 layers by critically investigating dc transport and more importantly, ac transport measurements, and show that the electrical performance of large area CVD-grown MoS_2 layers are extremely similar to mechanically exfoliated samples from naturally occurring crystals. Our observations indicate that atomically thin CVD MoS_2 layers show "universal" ac features, with the real part of the ac conductivity [$\sigma'(\omega)$] constant at low frequencies but following an approximate power law $\sigma'(\omega) \sim \omega^s$ at high frequencies. The exponent "s" has a weak temperature dependence and is close to unity within the studied range of 10 K $< T <$ 340 K. The weak temperature dependence of "s" indicates that the ac conduction occurs via quantum-mechanical tunneling (QMT) processes of electrons and is typically observed in highly crystalline and commercially available MoS_2 [20]. Finally, we show that these samples follow the "time-temperature superposition principle" (TTSP), as indicated by the collapse of the ac conductivity data onto a single master curve through proper scaling.

Large area MoS_2 layers were synthesized through the CVD technique on SiO_2 substrates. The process involves a direct chemical reaction between Mo and S and is described elsewhere [13] in detail. The topographical homogeneity of the samples was measured using atomic force microscopy (AFM, Agilent PicoScan 5500). Raman spectroscopy (Renishaw inVia), with a 514.5-nm laser excitation wavelength and a power of 2 mW, was used to characterize the structure and the number of layers of the films. These large area flakes were electrically contacted on top using patterns of Au with an underlying Ti layer through standard photo lithography techniques. The ac transport properties were measured (under high vacuum; pressure $<10^{-5}$ Torr) from 10 mHz to 0.1 MHz within a temperature range of 10–340 K using a temperature-controlled helium cryostat (Janis, closed cycle) coupled to a potentiostat/galvanostat with a built-in frequency response analyzer at 10 μHz to 2 MHz (PARSTAT 2263, Princeton Applied Research). An ac amplitude of 1 V was applied between the contacts, and the response was recorded in the form of a standard Bode plot and a Nyquist plot. The dc transport measurements were performed using a Keithley source meter model no. 2410.

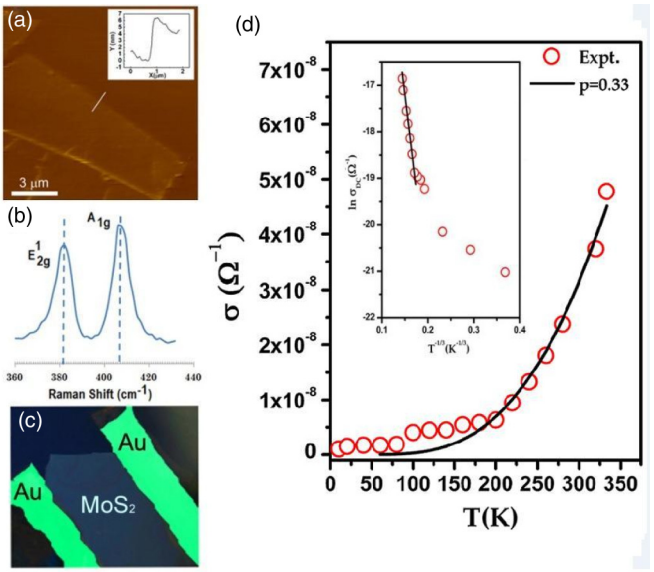

FIG. 1. (Color online) (a) AFM topography of typical CVD grown MoS_2 layers, (b) Raman spectrum of the sample, (c) psuedo-colored optical image of the device, and (d) temperature dependence of the dc conductivity are shown for CVD MoS_2. (Inset): ln σ_{dc} (y-axis) is plotted as a function of $T^{-1/3}$ (x-axis).

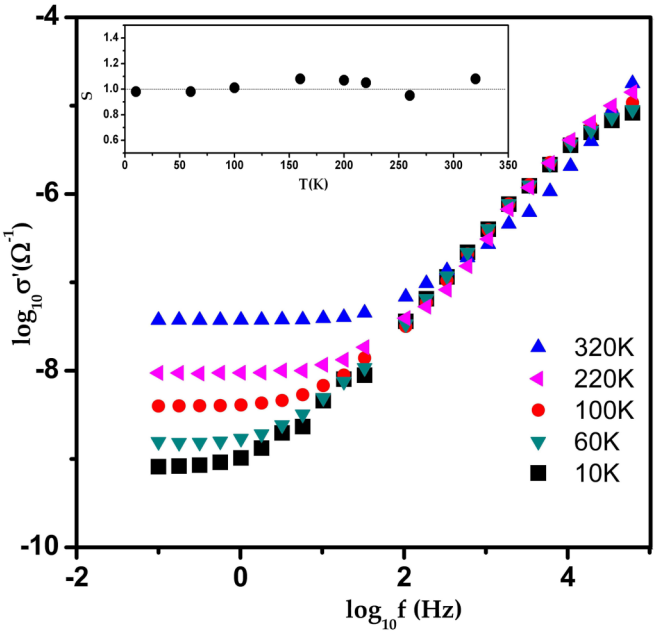

FIG. 2. (Color online) Frequency dependence of the real part of the ac conductivity at different temperatures for CVD grown MoS_2. log($\sigma'(\omega)$) is plotted as a function of the log of the frequency f. (Inset): Frequency exponent s as a function of the temperature. The dotted line is a guide to the eyes.

Figure 1 shows the structural and dc transport characterization of our sample. The AFM topography is shown in Fig. 1(a), and the Raman signal obtained for our MoS_2 samples, with peaks located at ~383 cm^{-1} [assigned to the in-plane vibration (E^1_{2g}) of sulfur and molybdenum atoms] and ~406 cm^{-1} [the out-of-plane vibrations (A_{1g} mode) of the sulfur atoms [29]], is shown in Fig. 1(b). The positions of these two peaks correspond to the MoS_2 sample composed of ~4–5 layers [13]. An optical image of a typical MoS_2 device, contacted with Ti/Au on top (two terminals), used for electrical transport measurements, is shown in Fig. 1(c). The temperature dependence of the dc conductivity is shown in Fig. 1(d). The mechanism of dc conduction can be extracted from the temperature dependence of the conductivity. For example, in many disordered systems, a power-law dependence on temperature is observed for the logarithm of the ohmic conductivity and is attributed to a conduction process driven by hopping between occupied and unoccupied localized states located between the valence and the conduction bands, the so-called variable range hopping (VRH) mechanism, first proposed by Mott and Davis [18]. The temperature dependence of the electrical conductivity in the VRH regime is expressed as

$$\sigma(T) = \sigma_0(T)\exp(-T_0/T)^p, \tag{1}$$

where $\sigma_0(T) \propto (1/T)^a$, $p = 1/(d+1)$. T_0 is a characteristic temperature and d is the dimensionality of the system. Thus, for a three-dimensional system $p = 1/4$, while for a two-dimensional system $p = 1/3$ (2D-VRH process). Furthermore, the temperature T_0 is related to the effective density of states near the Fermi level $N(E_F)$ as

$$T_0 = \frac{13.8\alpha^2}{k_B\, N(E_F)}, \tag{2}$$

where α and p are constants (α^{-1} is the localization distance) [18]. Therefore, in any given system, if 2D-VRH is responsible for the dc conduction mechanism, then ln(σ) should vary linearly with $1/T^3$. Such behavior was indeed observed in the dc transport measurements performed on our samples [Fig. 1(d), inset]. We have calculated the characteristic temperature T_0 for MoS_2 samples by fitting the actual conductivity data with Eq. (1). From this fit we obtained the value of $T_0 \sim 1.01 \times 10^5$ K, which is sufficiently higher than the temperature window of the measurement (60–340 K). Thus, we can conclude that for temperatures ranging from 60 to 333 K, and in CVD-grown layers of MoS_2, the 2D-VRH is the predominant conduction mechanism. Here, it is important to emphasize that such behavior was also observed in highly crystalline, few-layered samples of mechanically exfoliated MoS_2 with values of $T_0 \sim 10^4 - 10^6$ K [19]. To gain further insight into the nature of the conduction mechanism, we also measured the ac conductivity of MoS_2 samples. Figure 2 shows the logarithm of the real part of the ac conductivity (σ') as a function of the logarithm of the frequency f ($f = \frac{\omega}{2\pi}$) at selected temperatures. Several pieces of information related to the dependence of σ' on frequency can be drawn from this data: (i) σ' remains constant up to a certain frequency f_c; (ii) f_c decreases with decreasing temperature; and (iii) for $f > f_c$, σ' follows a power-law dependence of the form $\sigma' \propto f^s$. These observations indicate that the frequency-dependent conductivity in CVD-grown, large area MoS_2 can be explained on the basis of a universal ac conduction expression seen in a variety of disordered solids [18,21,23,24]:

$$\sigma'(\omega) = \sigma_0 + A\omega^s, \tag{3}$$

where $\sigma'(\omega)$ is the real part of the conductivity, including the frequency-dependent conductivity under an ac field, σ_0 is the dc or the low-frequency conductivity, A is a constant (weakly dependent on temperature), ω is the angular frequency of the applied field, and s is the frequency exponent. The variation of s with temperature for a variety of disordered materials was extensively analyzed in the past and is shown to be critically dependent on the ac conduction mechanism [20–25]. For example, in cases where the conductivity is believed to be due to phonon-assisted tunneling between defect states, or the so-called quantum-mechanical tunneling (QMT) phenomena, the ac conductivity $\sigma'(\omega)$ takes the functional form [18,20–28]

$$\sigma'(\omega) = ce^2 k_B T a[N(E_F)]^2 \omega R_\omega^4, \tag{4}$$

where $c = \frac{\pi}{24}$ is a constant, e is the elementary charge, $N(E_F)$ is the density of states at the Fermi level, and R_ω is the tunneling distance at a particular frequency given by

$$R_\omega = \frac{1}{2\alpha} \ln\left(\frac{\Gamma_0}{\omega}\right), \tag{5}$$

with Γ_0 being the phonon frequency $\sim 10^{13}$ Hz. The exponent s can be determined through $s = d\ln(\sigma)/d\ln(\omega)$ and it takes the form

$$s = 1 - \frac{4}{\ln(\Gamma_0/\omega)}. \tag{6}$$

It is important to emphasize that s is independent of temperature in the QMT model.

The dependence of s on temperature is shown in the inset of Fig. 2. It is clear from the data that $s \sim 1$ and is weakly dependent on T within the studied temperature range (10 K $< T <$ 340 K), which is a strong indication for the occurrence of the QMT phenomena. A critical analysis of the effect of the structural order on both dc and ac transport mechanisms was performed by Belougnea *et al.* [20] in thermally treated MoS_2 powders, as well as in commercially available polycrystalline MoS_2 flakes. The authors found that the behavior of both the dc as well as the ac transport correlates strongly with the degree of disorder in the investigated MoS_2 samples. It was shown that for highly disordered samples, $\ln(\sigma_{dc})$ follows a $1/T$ dependence with a temperature-dependent exponent s for the frequency f. A temperature-dependent "s" arises from processes where the charge carriers hop between defects, overcoming the potential barrier separating them, and therefore it can be explained by the correlated barrier hopping (CBH) mechanism. On the other hand, thermally annealed MoS_2 showing an improved crystallinity, as well as commercially available polycrystalline samples, displayed $\ln(\sigma_{dc}) \sim 1/T^3$ and a T-independent s, similar to the results obtained in the case of large area CVD-grown MoS_2. In Table I we list and compare several physical parameters related to the transport properties of the CVD-grown MoS_2 samples studied here and obtained from commercially available samples [20].

We have further observed that it is possible to scale the ac conductivity data for the MoS_2 sample using the formalism developed by Almond *et al.* [30]. In this formalism the ac conductivity is given by

$$\frac{\sigma'}{\sigma_0} = 1 + \left(\frac{f}{f_c}\right)^n, \tag{7}$$

TABLE I. Relevant physical parameters for MoS_2 as extracted by correlating the experimental transport properties with available theoretical models.

Sample	CVD	Commercial [20]
Model	QMT	QMT
"s"	1.0	0.73
σ_{dc}	$\sim T^{-1/3}$	$\sim T^{-1/3}$
$N(E_F)$	1.38×10^{21} eV^{-1} cm^{-3} @ 1 kHz (320 K)	1.16×10^{19} eV^{-1} cm^{-3} (300 K)

where n is a constant and f_c is a characteristic frequency, i.e., an onset frequency beyond which the conductance becomes frequency dependent. The plot of the normalized conductivity σ'/σ_0 with respect to the reduced frequency f/f_c forces all the data to collapse onto a single master curve [also referred to as the time-temperature superposition principle (TTSP)] [22,26,31]. We found that our CVD MoS_2 sample follows a scaling behavior which is consistent with this formalism (see Fig. 3). Under the TTSP, f_c scales with the low-frequency conductivity σ_0 as $f_c = A\sigma_0^x$. The values of x for different disordered systems are found to be of the order of the unity. This is a consequence of the Barton–Nakajima–Namikawa (BNN) relation, which is given by $\sigma_0 = p\Delta\varepsilon\varepsilon_0 2\pi f_c$, where p is a numerical constant of the order of unity, and $\Delta\varepsilon$ is the dielectric loss strength which displays a weaker temperature dependence than f_c (or σ_0), therefore implying that $f_c \sim \sigma_0$, or that $x \simeq 1$. From our measurements we found that $f_c \sim \sigma_0^x$, with the exponent $x = (0.95 \pm 0.04)$ (see inset of Fig. 3).

Finally, in order to ensure that our measurements were free from spurious effects arising, for example, from contact resistance and/or capacitance, we have performed impedance spectroscopy (IS) measurements at several temperatures. The IS data obtained at 320 K is shown in Fig. 4. To capture

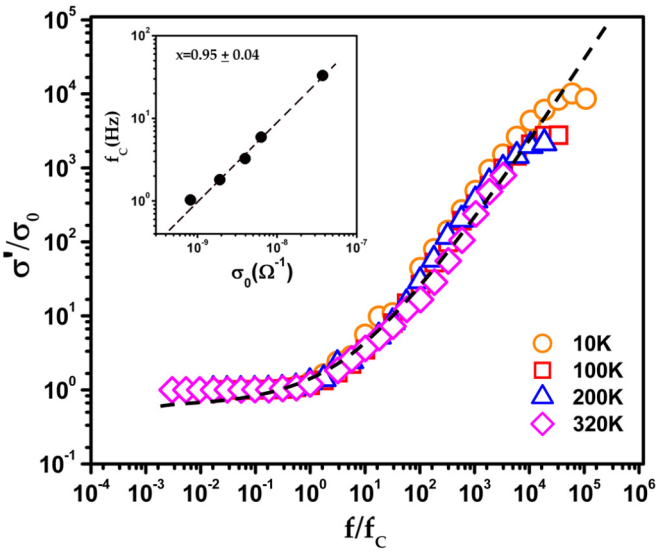

FIG. 3. (Color online) Scaling of the ac conductivity measured at different temperatures for CVD-grown MoS_2. (Inset): f_c as a function σ_0. Dotted lines are guides to the eyes.

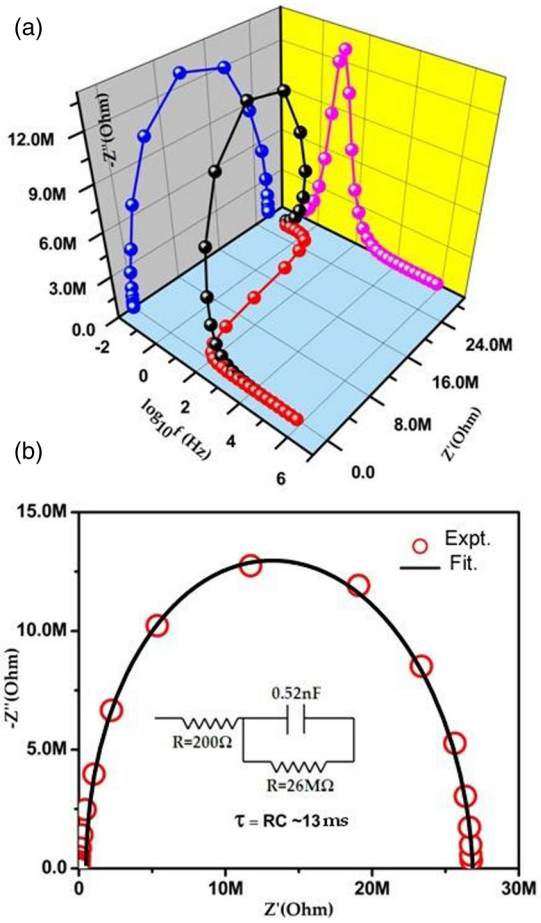

FIG. 4. (Color online) Three-dimensional plot of the impedance $Z = Z' + iZ''$ at 320 K. It shows a single frequency peak in the plane defined by Z'' as a function of $\log f$ (magenta markers). (b) The equivalent circuit which models the overall behavior of the impedance data.

the essence of the complete response in a single graph, we plotted a three-dimensional perspective of the impedance $Z(f)$ in Fig. 4(a). This figure shows the variation of the complex component of the impedance (Z'') with respect to the logarithm of the frequency ($\log f$) as well as the measured real part of the impedance Z'. Notice that the variation of Z'' as a function Z' (i.e., Cole-Cole plot) follows a single semicircular arc, indicating a Debye-like process dominated by a single relaxation time τ [32,33].

The Z'' as a function of $\log f$ plot reveals a single dielectric loss peak at $f_c \sim 10$ Hz which coincides with the onset frequency for the ac conduction. An equivalent circuit which models the Cole-Cole plot yields $\tau \sim 13$ ms [Fig. 4(b)]. The low-frequency intercept, i.e., the right side of the single arc, was also found to yield a value of real impedance Z', similar to the value obtained from the dc measurement on the sample at that particular temperature. The existence of a single time constant, together with the absence of any secondary semicircular arc in the Cole-Cole plot at lower frequencies, indicates that the whole polarization mechanism arises from the semiconducting grains of MoS_2.

In conclusion, we have performed a detailed study and concomitant analysis on the electrical transport properties of large area CVD-grown MoS_2. The CVD synthesis is a low-temperature process. Therefore defects and disorder are inherent to the materials grown through this process and it is expected that $\sigma_{dc} \sim \exp(T^{-1})$ and $\sigma'(\omega) = A\omega^s$, with a T-dependent s [20]. On the contrary, our measurements show that in CVD-grown, large area MoS_2, $\sigma_{dc} \sim \exp(T^{-1/3})$ and $\sigma'(\omega) \sim \omega^s$ (with a *T-independent s*). The combination of dc and ac conductivity analysis shows that in these atomically thin layers the electrical conduction results from electronic hopping between localized states near the Fermi level, as predicted by the QMT model, typically observed in highly crystalline MoS_2. Therefore, we conclude that large area, CVD-grown MoS_2 are equivalent in their electrical transport properties of highly crystalline MoS_2 and are good candidates for niche electronics and optoelectronics applications. We believe that these findings not only advance our fundamental understanding of the transport mechanism in few-layered, CVD-grown MoS_2 systems, but will also motivate the need to critically investigate the transport mechanisms in other 2D layered systems.

This work is supported by the US Army Research Office, MURI Award No. W911NF-11-1-0362. J.L. acknowledges support from the Welch Foundation, Grant No. C-1716, and the NSF-ECCS, Grant No. 1327093. S.K. acknowledges financial support under the NSF ECCS, Grant No. 1351424.

[1] K. S. Novoselov, D. Jiang, F. Schedin, T. J. Booth, V. V. Khotkevich, S. V. Morozov, and A. K. Geim, Proc. Natl. Acad. Sci. USA **102**, 10451 (2005).
[2] B. Radisavljevic, A. Radenovic, J. Brivio, V. Giacometti, and A. Kis, Nat. Nanotechnol. **6**, 147 (2011).
[3] J. N. Coleman, M. Lotya, A. O'Neill, S. D. Bergin, P. J. King, U. Khan, K. Young, A. Gaucher, S. De, R. J. Smith *et al.*, Science **331**, 568 (2011).
[4] T. Bjorkman, A. Gulans, A. V. Krasheninnikov, and R. M. Nieminen, Phys. Rev. Lett. **108**, 235502 (2012).
[5] Q. H. Wang, K. Kalantar-Zadeh, A. Kis, J. N. Coleman, and M. S. Strano, Nat. Nanotechnol. **7**, 699 (2012).
[6] S. Kim, A. Konar, W.-S. Hwang, J. H. Lee, J. Lee, J. Yang, C. Jung, H. Kim, J.-B. Yoo, J.-Y. Choi *et al.*, Nat. Commun. **3**, 1011 (2012).
[7] Y. Zhang, J. Ye, Y. Matsuhashi, and Y. Iwasa, Nano Lett. **12**, 1136 (2012).
[8] Z. Yin, H. Li, H. Li, L. Jiang, Y. Shi, Y. Sun, G. Lu, Q. Zhang, X. Chen, and H. Zhang, ACS Nano **6**, 74 (2012).
[9] H. S. Lee, S-W. Min, Y-G. Chang, M. K. Park, T. Nam, H. Kim, J. H. Kim, S. Ryu, and S. Im, Nano Lett. **12**, 3695 (2012).
[10] G. Eda, H. Yamaguchi, D. Voiry, T. Fujita, M. Chen, and M. Chhowalla, Nano Lett. **11**, 5111 (2011).

[11] R. J. Smith, P. J. King, M. Lotya, C. Wirtz, U. Khan, S. De, A. O'Neill, G. S. Duesberg, J. C. Grunlan, G. Moriarty *et al*., Adv. Mater. **23**, 3944 (2011).
[12] A. Castellanos-Gomez, M. Barkelid, A. M. Goossens, V. E. Calado, H. S. J. van der Zant, and G. A. Steele, Nano Lett. **12**, 3187 (2012).
[13] Y. Zhan, Z. Liu, S. Najmaei, P. M. Ajayan, and J. Lou, Small **8**, 966 (2012).
[14] Y.-H. Lee, X.-Q. Zhang, W. Zhang, M.-T. Chang, C.-T. Lin, K.-D. Chang, Y.-C. Yu, J. T.-W. Wang, C.-S. Chang, L.-J. Li *et al*., Adv. Mater. **24**, 2320 (2012).
[15] K.-K. Liu, W. Zhang, Y.-H. Lee, Y.-C. Lin, M.-T. Chang, C.-Y. Su, C.-S. Chang, H. Li, Y. Shi, H. Zhang *et al*., Nano Lett. **12**, 1538 (2012).
[16] W. Zhou, X. Zou, S. Najmaei, Z. Liu, Y. Shi, J. Kong, J. Lou, P. M. Ajayan, B. I. Yakobson, and J. Idrobo, Nano Lett. **13**, 2615 (2013).
[17] S. Najmaei, Z. Liu, W. Zhou, X. Zou, G. Shi, S. Lei, B. I. Yakobson, J. C. Idrobo, P. M. Ajayan, and J. Lou, Nat. Mater., **12**, 754 (2013).
[18] N. F. Mott and E. A. Davis, *Electronic Processes in Non-Crystalline Materials* (Clarendon Press, Oxford, 1971).
[19] S. Ghatak, A. N. Pal, and A. Ghosh, ACS Nano **5**, 7707 (2011).
[20] P. Belougnea, J. C. Giuntinia, and J. V. Zanchetta, Philos. Mag. B **53**, 233 (1986).
[21] S. Baranovski, *Charge Transport in Disordered Solids with Applications in Electronics* (John Wiley, New York, 2006).
[22] J. C. Dyre and T. B. Schroder, Rev. Mod. Phys. **72**, 873 (2000).
[23] S. R. Elliott, Adv. Phys. **36**, 135 (1987).
[24] A. R. Long, Adv. Phys. **31**, 553 (1982).
[25] M. Pollak and T. H. Geballe, Phys. Rev. 122 (1961).
[26] T. B. Schroder and J. C. Dyre, Phys. Rev. Lett. **84**, 310 (2000).
[27] B. Roling, A. Happe, K. Funke, and M. D. Ingram, Phys. Rev. Lett. **78**, 2160 (1997).
[28] D. L. Sidebottom, Phys. Rev. Lett. **82**, 3653 (1999).
[29] C. Lee, H. Yan, L. E. Brus, T. F. Heinz, J. Hone, and S. Ryu, ACS Nano **4**, 2695 (2010).
[30] D. P. Almond, G. K. Duncan, and A. R. West, Solid State Ionics **8**, 159 (1983).
[31] J. C. Dyre, Phys. Rev B **47**, 9128(R) (1993).
[32] J. R. McDonald, Ann. Biomed. Eng. **20**, 289 (1992).
[33] Jin-Ha Hwang, K. S. Kirkpatrick, T. O. Mason, and E. J. Garboczi, Solid Sate Ionics **98**, 93 (1997).